All-Vacuum Processing for Fabrication of Efficient, Large-Scale and Flexible Inverted Perovskite Solar Cells

Mohammad Mahdi Tavakoli,[1,2]* *Rouhollah Tavakoli*[2]

[1]*Department of Electrical Engineering and Computer Science, Massachusetts Institute of Technology, Cambridge, 02139 MA, USA*

[2]*Department of Materials Science and Engineering, Sharif University of Technology, 14588 Tehran, Iran*

* Corresponding author: mtavakol@mit.edu

Abstract

Vacuum deposition of transporting layers, especially hole transporting layer (HTL) is still a big challenge for the fabrication of large-area perovskite solar cells (PSCs). Here, we fabricate efficient and large-area PSCs using an inverted architecture and evaporate all the transporting layers in a thermal evaporation vacuum chamber. In this work, we employ poly(bis(4-phenyl)(2,4,6-trimethylphenyl)amine) (PTAA) as HTL and successfully deposit a compact layer of PTAA with low thickness (2-10 nm), for the first time, using thermal evaporation. Our optical and ultraviolet photoelectron spectroscopy (UPS) measurements prove that the evaporated PTAA has a great match with the single A-cation methylammonium triiodide perovskite film in terms of quenching effect and band alignment. After fabrication of the inverted architecture using all vacuum processing, PSCs with power conversion of efficiencies (PCEs) of 19.4% for small area (0.054 cm^2) and 18.1 % for large-area (1 cm^2) are achieved, which are higher than those of solution-based devices. We also fabricate flexible PSC with PCE of 17.27% using this approach. Moreover, the fabricated PSCs using vacuum technique show negligible hysteresis and good stability, better than

This is the author manuscript accepted for publication and has undergone full peer review but has not been through the copyediting, typesetting, pagination and proofreading process, which may lead to differences between this version and the Version of Record. Please cite this article as doi: 10.1002/pssr.202000449.

the devices fabricated on the spin-coated PTAA. This work highlights the potential of vacuum deposition for scale-up and commercialization of the PSCs.

Keyword: Perovskite, Solar cell, PTAA, Vacuum deposition, efficiency

Introduction

Unique optoelectronic properties of organometal halide perovskites with ABX_3 (A: MA, FA, Cs; B: Pb,Sn; C: I,Br,Cl) crystal structure make them ideal candidates for the fabrication of high efficiency solar cells.[1-8] During the past years, extensive efforts have been devoted to improving the efficiency and stability of the perovskite solar cells (PSCs) by considering compositional engineering, interface engineering, additive engineering, and passivation techniques.[9-17] These approaches lead to a certified power conversion efficiency (PCE) of 25.2%, which surpasses the record of all thin film solar cells.[18,19] In order to fabricate PSCs, there are two approaches for the fabrication of device, i.e., solution processing and vacuum deposition.[20-23] Both approaches have great potential for fabrication of PSCs with PCE over 20%, however, for scale-up and commercialization purposes, vacuum technique has a better potential due to its precise control on the deposition in large area.[24,25] Vacuum techniques such as chemical vapor deposition (CVD),[26] thermal evaporation in one-step[27] or two-step[28], and layer-by-layer deposition[29,30] have great advantages over solution processing including fabrication of high quality and pinhole-free perovskite film with excellent uniformity and surface coverage, solvent-free processing, reproducibility, scalability, substrate-independent for deposition, and the potential for purification of precursors before deposition.[31-35]

In order to fabricate PSCs with all vacuum processing, not only perovskite film but also all transporting layers should be deposited by a vacuum method. Regarding electron transporting layer (ETL), high quality metal oxides such as SnO_2, TiO_2, ZnO, etc can be deposited by sputtering.[36] However, using thermal evaporation, the quality of these ETLs may not be good enough for high efficiency device. To address this issue and deposition of all layers by thermal evaporation technique, C60 or other organic ETLs with evaporation capability need to be employed.[37,38] In fact, for the fabrication of all vacuum

PSCs with high efficiency, HTL is usually the limiting factor and there are only few choices for this purpose such as NiO,[39,40] which are not good enough for the fabrication of high efficiency device. In this regard, Hsiao *et al.*[41] fabricated all vacuum PSC with a normal architecture of ITO/C60/$CH_3NH_3PbI_3$/4,4′-cyclohexylidenebis[*N*,*N* -bis(4-methylphenyl)benzenamine](TAPC)/TAPC:MoO_3/MoO_3/Ag. They reported PSCs with PCE of up to 17.6%, which is among the best reported value. Gil-Escrig et al.[42] fabricated PSCs with device structure of ITO/C60:Phlm/C60/mixed cation perovskite/TaTm/TaTm:F_6-TCNNQ/Au using all vacuum processing and reported PCE of up to 16%. In another similar work, Longo et al.[43] employed the same device architecture as the previous work but different perovskite, $MAPb(Br_{0.2}I_{0.8})_3$ and obtained PCE of up to 15.9%. All of the reported devices in the literature employed normal architecture starting from ETL and the PCE is still far away from the state of art in the literature. Therefore, more efforts are required here to further push the PCE of all-vacuum processing PSCs.

In this work, for the first time, we report all-vacuum processing PSCs using an inverted structure by using only thermal evaporation technique for all layers. We employ PTAA as HTL and evaporate an ultrathin layer (optimum thickness: 4 nm) of PTAA on ITO glass. Then, the perovskite film is deposited on HTL using a layer-by-layer evaporation technique, which provides us a high quality and uniform perovskite film. To complete the device structure, C60 as ETL, bathocuproine (BCP) as buffer layer, and silver as electrode were thermally evaporated on perovskite film. Using this structure, PSCs with PCEs of 19.4% and 18.1% are achieved for small and large area devices, respectively, which are among the best reported value in the literature. Moreover, we fabricate flexible PSC on Polyethylene terephthalate (PET)/ITO substrate and obtain a PCE of 17.27% with a good mechanical property using this approach. Additionally, our devices fabricated by all-vacuum method show negligible hysteresis with good stability.

Results and Discussion

In order to evaluate the possibility of PTAA evaporation, we first performed gel permeation chromatography (GPC) test for the PTAA before and after evaporation, as shown in Figure S1. From this measurement, the average molecular weight (Mw) of the PTAA before and after evaporation were obtained to be 16.02 kDa and 15.97 kDa, respectively. This indicates that the M_W of PTAA and possibly its molecular structure are not changed by evaporation. Notably, the M_W of our PTAA purchased from the EM Index company is much smaller than the PTAA from other company such as the one from Sigma Aldrich (45 kDa). Figure 1a shows the transmittance spectra of the spin-coated and evaporated PTAA films. As seen, the transmittance and absorption edge of PTAA in both cases are almost identical, indicating an average visible transmittance of over 80% and a bandgap of 3.5 eV. Figures 1b and 1c depict the atomic force microscopy (AFM) images of the PTAA films, deposited by solution and evaporation approaches. The average roughness for the evaporated PTAA film (1.6 nm) is slightly lower than that of the solution based PTAA (2.5 nm), as can be seen in Figure S2. This indicates slightly more smoothness of the evaporated PTAA film, which is beneficial for large-scale fabrication. In order to study the charge transfer property of the PTAA films, methylammonium lead triiodide ($MAPbI_3$) perovskite film was thermally evaporated on PTAA HTLs using a layer-by-layer deposition technique (Figure S3).[30]

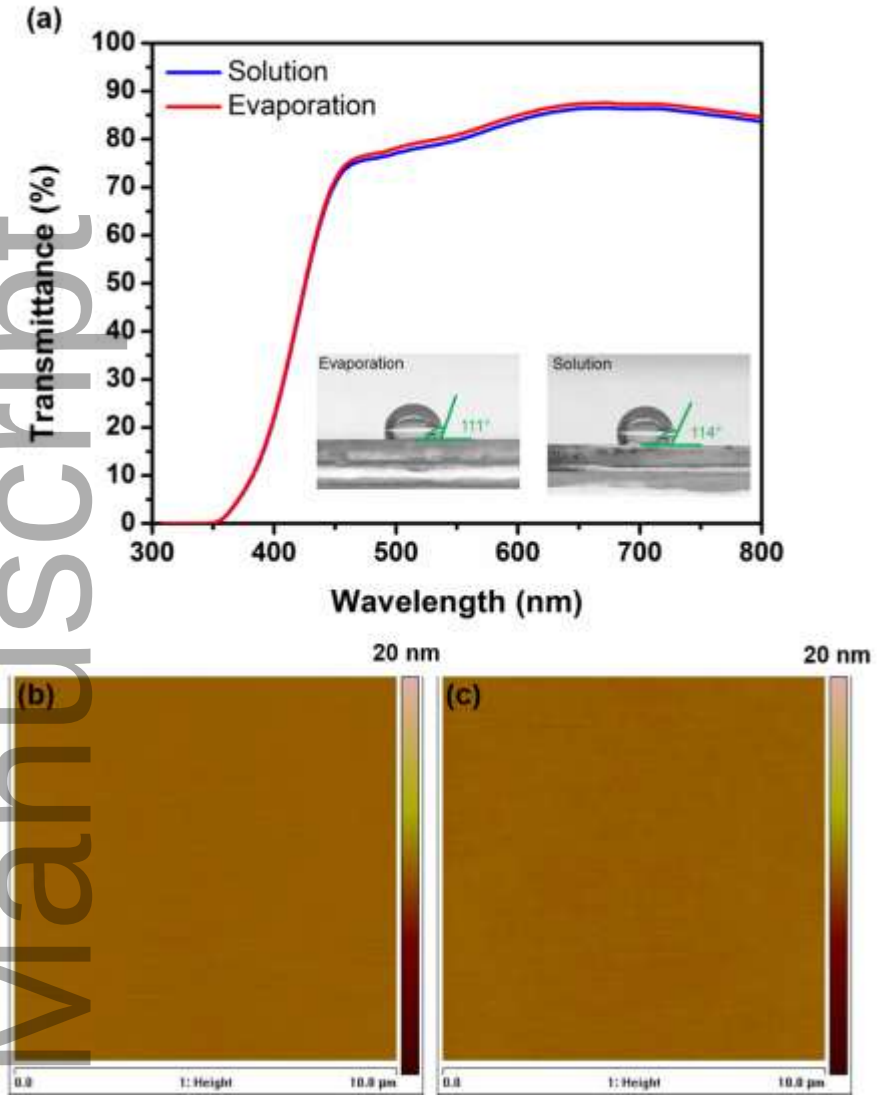

Figure 1. (a) Transmittance spectra of PTAA films deposited by spin-coating and evaporation methods. The inset images are the contact angles of DMF droplet on the surface of the corresponding films. AFM images of the PTAA films deposited by (b) evaporation and (c) spin-coating approaches.

Top-view scanning electron microscopy (SEM) images of the perovskite films deposited on spin-coated and evaporated PTAA are shown in Figures 2a and 2b, respectively. As can be observed, the perovskite films have good crystallinity in both cases, however, the perovskite on the evaporated PTAA shows slightly larger grain size. This could be corresponded to the solvent effect (the residual Toluene molecules left after spin-coating of the PTAA) and the surface quality of the PTAA. To further study the surface of PTAA in both methods, AFM images of both films were

studied as shown in Figure S4. From the AFM images, the perovskite film on the evaporated PTAA shows also slightly larger grain size, which is in good agreement with SEM images. Moreover, we find that the surface roughness of the perovskite film on the spin-coated PTAA is 25±4 nm, which is higher than that of perovskite film on the evaporated PTAA (16±3 nm). The surface roughness of the perovskite film can induce surface recombination at HTL/perovskite interface, resulting in lower open circuit voltage (V_{OC}).[44-46] The crystallinity of the perovskite films deposited on solution and evaporation based PTAA was investigated by x-ray diffraction pattern (XRD), as can be found in Figure S5. As seen, the perovskite film on the evaporated PTAA film shows peaks with slightly higher intensity, indicating better quality of the perovskite in this sample.

The optical properties of the corresponding perovskite films were further studied by UV-visible and photoluminescence (PL) spectroscopies. Figure 3c shows the UV-Visible spectra of both films, indicating a bandgap of 1.55 eV in both cases. The PL spectra of both samples shown in Figure 3d depict the quenching effect of perovskite film deposited on both PTAA HTLs. As seen, the perovskite film on the evaporated PTAA demonstrates stronger quenching effect as compared to the spin-coated one, confirming the better hole transfer property in this sample. We also confirm this behavior by using time-resolved PL (TRPL) measurement, as shown in Figure 3e. The fitting parameters (using biexponential equation) can be found in Table S1. From the lifetime measurements, we can conclude that the perovskite film deposited on the evaporated PTAA has stronger quenching effect and thus better hole transfer property compared with the spin-coated sample.

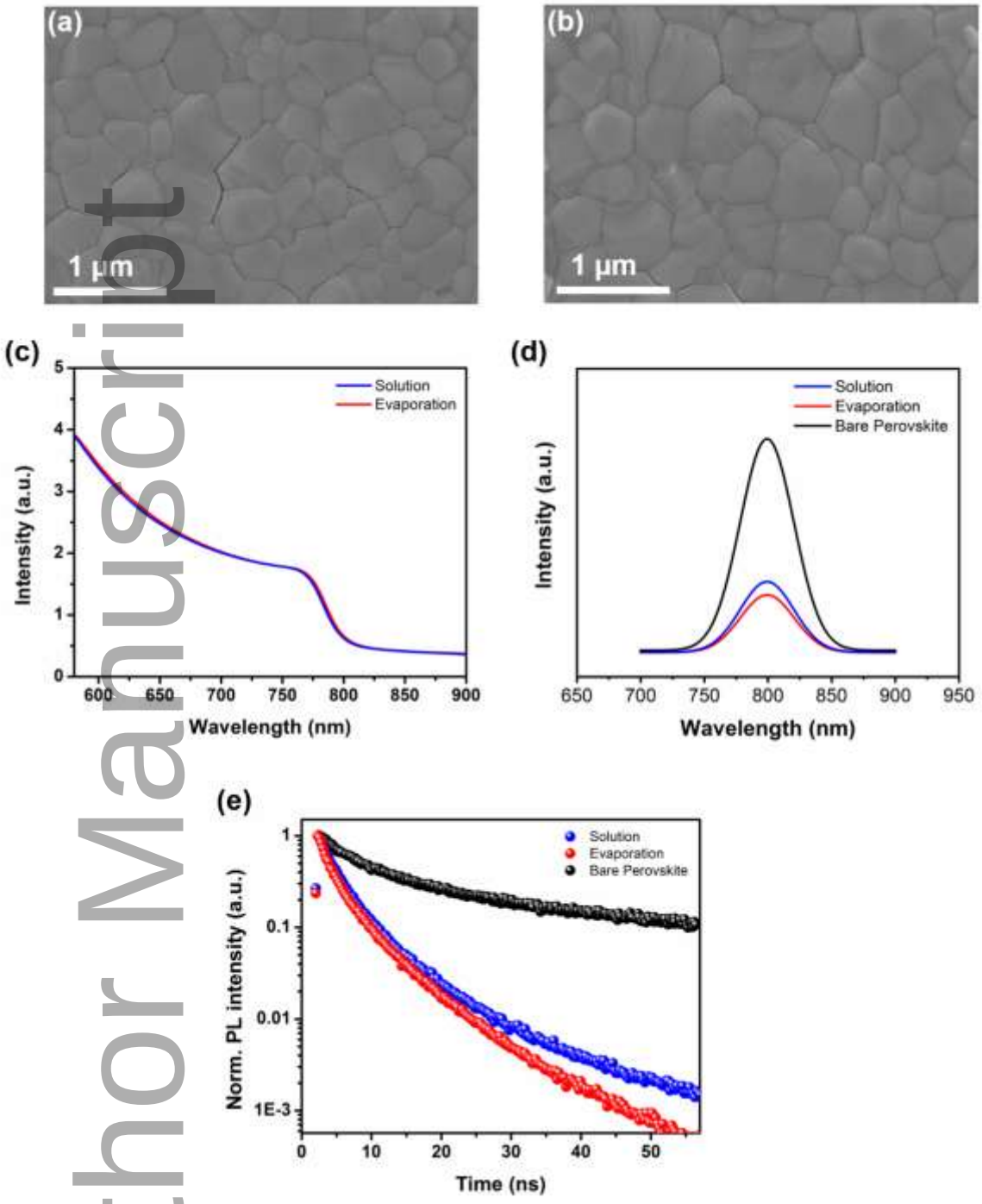

Figure 2. Top-view SEM images of the perovskite film deposited on spin-coated (a) and evaporated (b) PTAA HTLs. (c) UV-Visible and (d) PL spectra of the perovskite films, deposited on spin-coated and evaporated PTAA HTLs. (e) TRPL spectra of the bare perovskite and perovskites on the corresponding PTAA HTLs.

In order to investigate the photovoltaic (PV) properties of the representative PTAA HTLs, perovskite solar cells with inverted architecture were fabricated. Figure 3a and 3b shows the cros-

sectional SEM image and schematic of the device, respectively. As seen, the device is consisted of indium-doped tin oxide (ITO) glass, PTAA HTL, perovskite film, C60 as electron transporting layer (ETL), bathocuproine (BCP) as buffer layer, and silver (Ag) as electrode. All layers here were deposited by thermal evaporation technique and we selected single A-cation perovskite, i.e., $MAPbI_3$ for this study. Figure 3c shows the current density-voltage (J-V) curves of the representative PSCs measured under standard condition (AM1.5G) and reverse bias. The PV results, summarized in Table 1, indicate a PSC fabricated on spin-coated PTAA with a short circuit current density (J_{SC}) of 23.02 mA/cm^2, a V_{OC} of 1085 mV, a fill factor of 73% and a maximum PCE of 18.3 %. While by fabrication of device on the evaporated PTAA, a PSC with maximum PCE of 19.4% (J_{SC} of 23.11 mA/cm^2, V_{OC} of 1090 mV and FF of 77%) is achieved. This value is the best reported PCE in the literature for all-vacuum processing device, to the best of our knowledge. The maximum power point (MPP) tracking for both devices are measured and shown in Figure 3d, indicating stabilized PCEs of 18.15% for spin-coated and 19.22% for evaporated PTAA HTLs over 60 s. To validate the J_{SC} of the presented PSCs, external quantum efficiency (EQE) of the devices were measured as can be seen in Figure 3e. Both devices show EQE over 80% in the range of 350-750 nm. After integration of EQE by the solar spectrum, the J_{SC} of the PSCs were extracted to be 22.18 mA/cm^2 and 22.31 mA/cm^2 for the devices with spin-coated and evaporated PTAA, respectively. These values follow and confirm the trend of J_{SC} values obtained from J-V measurement. Figure S6 depicts the statistic of the PV parameters in the PSCs fabricated on spin-coated and evaporated PTAA HTLs. As seen, the average values of all PV parameters for the devices with the evaporated PTAA are higher than those of the devices with spin-coated PTAA, which is in good agreement with the J-V curves shown in Figure 3c. In fact, the difference in FF and V_{OC} is more intensive.

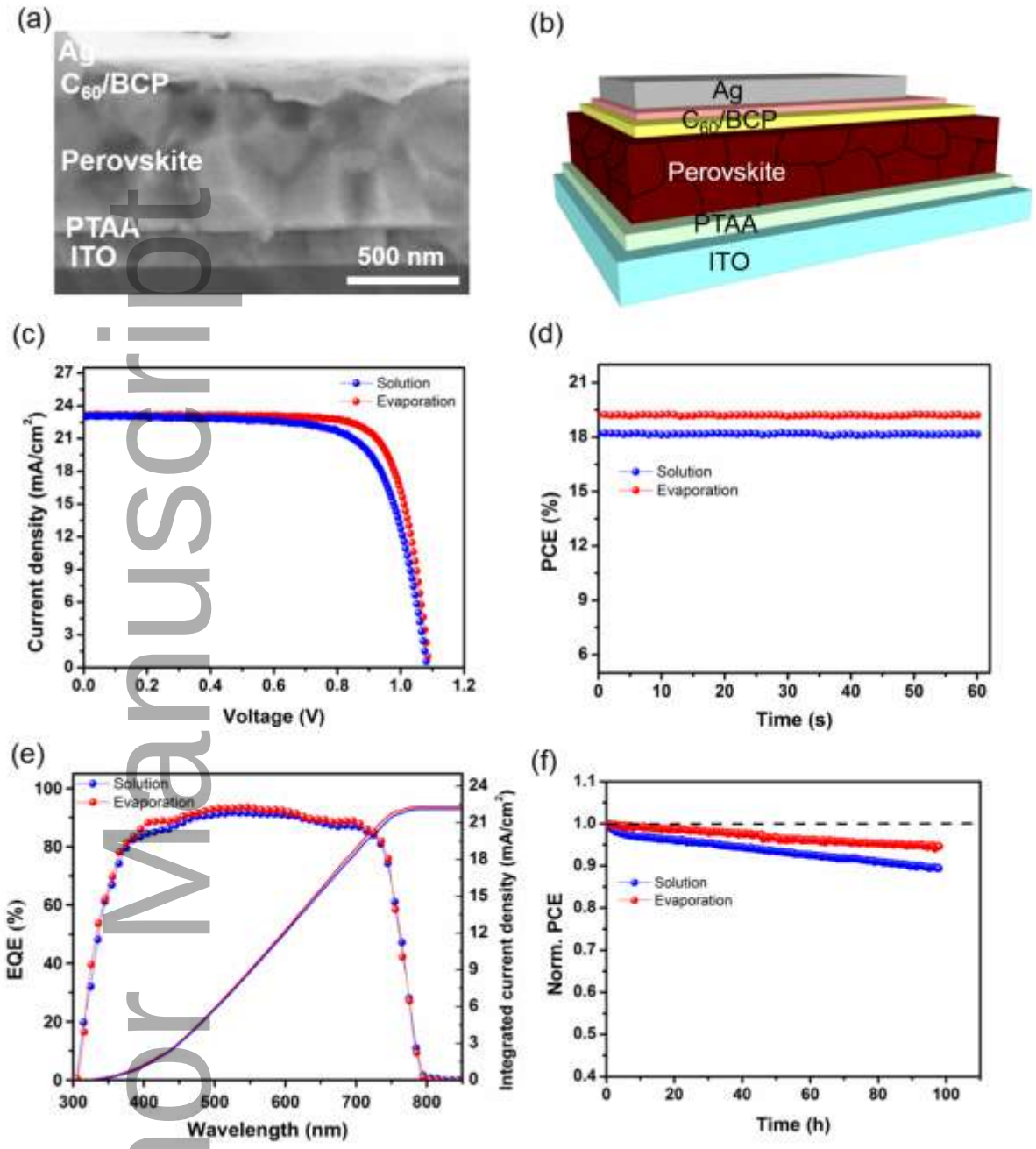

Figure 3. (a) Cross-sectional SEM image and (b) schematic of device architecture for the PSC devices fabricated on the evaporated PTAA. (c) J-V curves, (d) maximum power point tracking, and (e) EQE spectra of the PSCs fabricated on spin-coated and evaporated PTAA HTLs. (f) Operational stability measurement of the PSCs fabricated on spin-coated and evaporated PTAA HTLs.

Stability is the main challenge in the PSC field and need to be addressed before moving toward commercialization.[47] Therefore, we measured the stability of our PSCs under continuous illumination for 100 h, as shown in Figure 3f. The results show that the PSC with the evaporated

PTAA maintains 97% of its initial efficiency after 100 h under illumination, which is better than that of (89%) the device with spin-coated PTAA. This could be due to higher quality of the PTAA prepared by evaporation and lack of any residual solvent at the HTL/perovskite interface.

Beside the above results, we measured the average value of hysteresis index for both devices, as shown in Figure S7. Notably, the hysteresis index (HI) was calculated by the following formula:

$$HI\ (\%) = ((PCE_{backward} - PCE_{forward})/PCE_{forward}) \times 100$$

We find that the average value of HI for the evaporated PTAA is 1.25%, which is slightly lower than that of spin-coated one (1.55%). This can explain better charge transfer property of evaporated PTAA compared with spin-coated one. We also optimize the thickness of the evaporated PTAA as can be found in Figure S8. The PV results indicate that 4 nm-thick PTAA is the optimum thickness, which results in the highest efficiency. In fact, the optimum thickness of the solution-based PTAA layer is 8 nm, twice thicker than that of the evaporated-based PTAA film.[48]

In order to further study the improved PV parameters in the PSCs with the evaporated PTAA, ultraviolet photoelectron spectroscopy (UPS) measurement was performed in both cases. From the UPS results shown in Figure 4a, the valence bands of the PTAA films were estimated to be -5.2 eV and -5.31 eV for the spin-coated and evaporated samples, respectively. By considering the band alignment of the $MAPbI_3$ perovskite film from the literature,[49] we plotted the band diagram of the devices with both HTLs, as shown in Figure 4b. We find that the band offset at the PTAA/perovskite interface is only 90 meV for the evaporated PTAA, which is much lower than that of the spin-coated PTAA with 200 meV band offset. This can facilitate the hole transfer between the perovskite film and evaporated PTAA HTL and thus reduce the interface recombination, resulting in higher $V_{OC.}$[50,51] This result is in good agreement with the quenching effect observed from TRPL results. We also measured the dark I-V curves of the corresponding PSCs, as can be observed in Figure 4c. Our results indicate that the PSC with the evaporated PTAA

has smaller leakage current as compared to the one with the spin-coated PTAA, which can explain the higher V_{OC} in the device with evaporated PTAA.

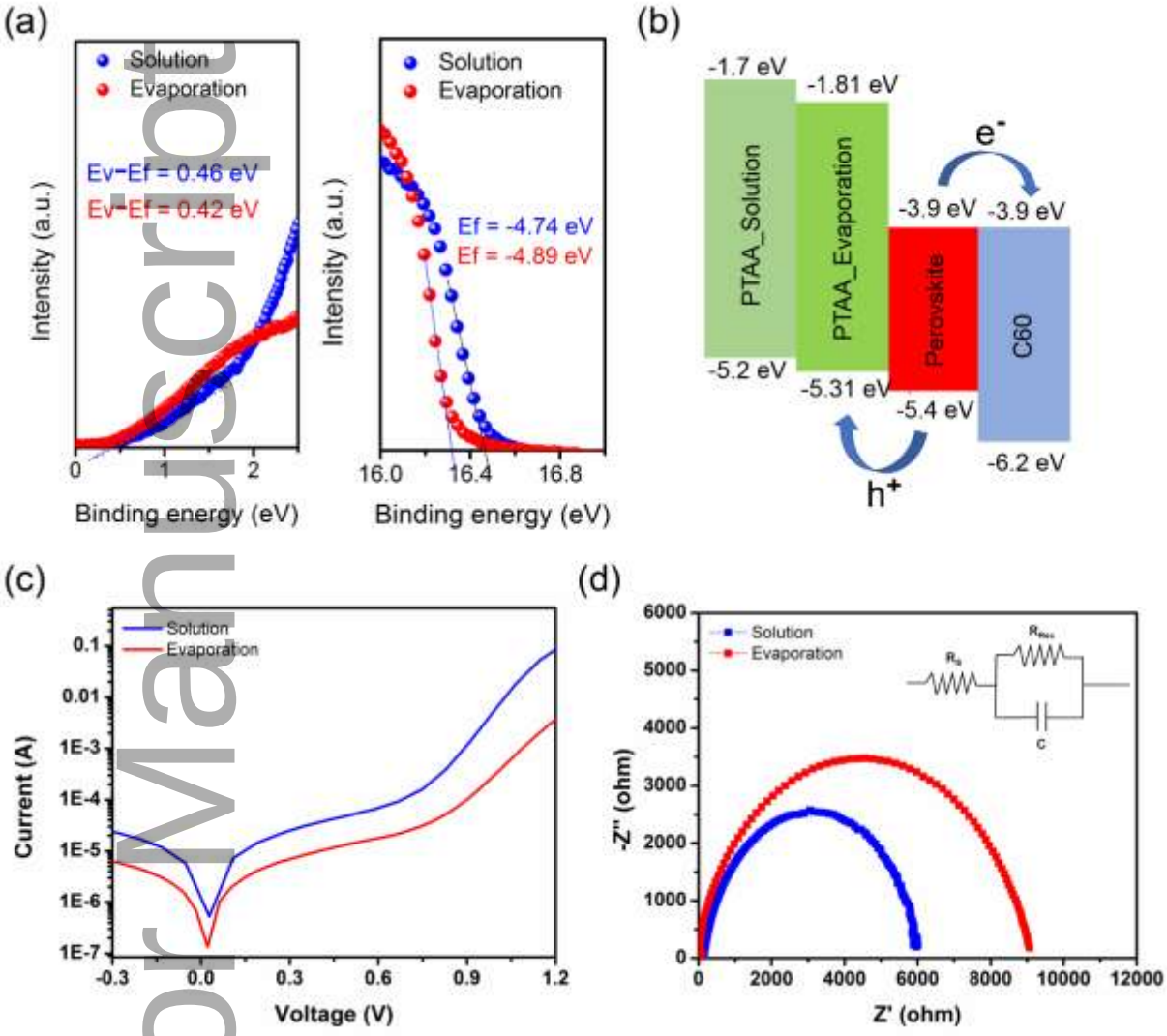

Figure 4. (a) UPS measurement of the PTAA HTLs deposited by spin-coating and evaporation methods. (b) Band diagram of the corresponding perovskite solar cells with both PTAA HTLs. (c) Dark I-V measurement and (d) Nyquist plots of the PSCs fabricated on spin-coated and evaporated PTAA HTLs. The inset image is the equivalent circuit for fitting of the curves.

In order to evaluate the role of HTL on the representative devices, electrochemical impedance spectroscopy (EIS) was measured with zero bias. Figure 4d shows the Nyquist plots of the PSCs with spin-coated and evaporated PTAA HTLs. The inset circuit shown in Figure 4d was employed to fit the EIS curves. In this circuit, R_S, $R_{Rec,}$ and C are series resistance, recombination resistance

and capacitance, respectively. The EIS results posit that the PSC fabricated on the evaporated PTAA has lower R_S (96 ohm) compared with the device with spin-coated PTAA (142 ohm). This can explain the higher FF in the device with the evaporated PTAA. Moreover, the device with evaporated PTAA shows higher recombination resistance, indicating the better PTAA/perovskite interface with lower interface recombination. The slightly higher V_{OC} in this device can be ascribed to the lower interface recombination.

To demonstrate the potential of all vacuum processing in the PSC field, we fabricate large-area (1 cm^2) and flexible PSCs. Figure 5a shows the J-V curves of the large-area PSCs fabricated on PTAA HTLs prepared by spin-coating and evaporation methods. The device with the evaporated PTAA indicates a PCE of 18.1% (J_{SC} of 22.9 mA/cm^2, V_{OC} of 1088 mV and FF of 72.6%), which is much better that the PSC fabricated on the spin-coated PTAA (15.02%). The inset graph displays the MPP curves of the corresponding devices over 60 s, indicating stable PCE over time for both cases. The statistics of J-V parameters, shown in Figure S9, clearly demonstrate the advantage of vacuum deposition of PTAA HTL. As seen, the average values of all PV parameters are improved using vacuum approach in large area, which can be ascribed to the poor uniformity of the spin-coated PTAA layer and also the solvent effect. Figure 5b shows the EQE spectra of the corresponding PSCs with large-area and the inset image in this figure shows the photograph of a large-area device with the evaporated PTAA. As seen in Table 1, the calculated J_{SC} from EQE curves are well-matched with the ones from the J-V results.

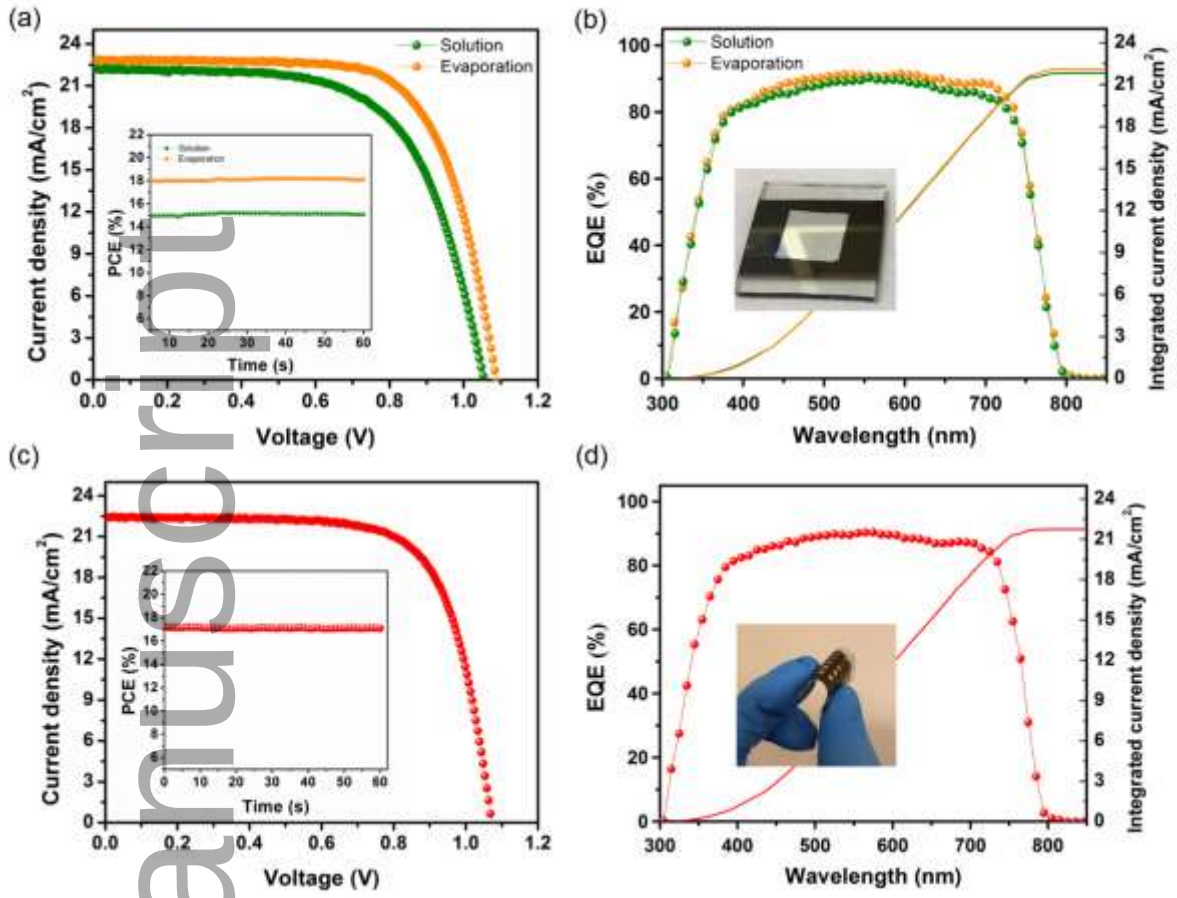

Figure 5. (a) J-V curves and (b) EQE spectra of the PSCs fabricated on spin-coated and evaporated PTAA HTLs with active area of 1 cm^2. The inset photograph in Figure 5b is the large-area device. (c) J-V curve and (b) EQE spectrum of the flexible PSC fabricated on PET substrate. The inset photo shows the flexible PSC using this configuration.

In addition to the large-area device, we demonstrate the application of all vacuum approach for the fabrication of flexible PSCs. Since the evaporated PTAA does not need any annealing, it would be a great choice for the flexible devices. However, for the spin-coated PTAA, annealing at temperatures over 100 °C is a mandatory step. Therefore, we used PET/ITO as flexible substrate and the PSC was fabricated on the evaporated PTAA HTL. Figure 5c and its inset graph show the J-V curve and MPP curve of the flexible PSC. Using this approach, we achieve a PCE of 17.27% (J_{SC} of 22.24 mA/cm^2, V_{OC} of 1071 mV and FF of 72 %), which is among the best performing flexible PSCs in the literature. We also validated the J_{SC} of this device using EQE measurement, as can be observed in Figure 5d and Table 1. The inset image in Figure 5d shows the flexible PSC fabricated on the

evaporated PTAA. Figure S10 shows the statistic of PV parameters for the flexible PSCs fabricated on the evaporated PTAA, indicating an average PCE of 16.82%. To evaluate the mechanical property of our flexible device, we performed a bending test by considering banding radiuses of 4 mm and 3 mm (Figure S11). We find that our flexible devices retain 85% and 57% of their initial PCE values with banding radiuses of 4 mm and 3 mm, respectively, after 100 bending cycles.

Table 1. Photovoltaic parameters of the champion inverted PSCs based on spin-coated and evaporated PTAA HTLs

Device (area (cm^2))	V_{oc} (mV)	J_{sc} (mA/cm^2)	FF (%)	PCE (%)	J_{sc} from EQE (mA/cm^2)
Solution (0.054)	1085	23.02	73	18.3	22.18
Evaporation (0.054)	1090	23.11	77	19.4	22.31
Solution (1.0)	1055	22.24	64	15.02	21.8
Evaporation (1.0)	1088	22.9	72.6	18.1	22.1
Flexible (0.054)	1071	22.4	72	17.27	21.7

Conclusions

In summary, we fabricate PSC devices with inverted architecture using all vacuum processing. We evaporate PTAA as an HTL for the first time in an inverted design and compare it with the solution-based PTAA. Our characterization results reveal that the evaporated PTAA is well-matched with $MAPbI_3$ perovskite film in terms of band alignment and even quenching effect, better than the solution-based PTAA. Here, we fabricate all the layers using thermal evaporation which is a great technique for commercialization. Based on this approach, we achieve maximum PCEs of 19.4% (0.054 cm^2) and 18.1% (1 cm^2) for the devices based on the evaporated PTAA, which shows better PV results and operational stability as compared to the PSCs with solution-based PTAA, particularly for the large-area device. We find that 4 nm-thick layer of PTAA is the optimum thickness in order to get the highest PCE. Device characterization results prove that the device on the evaporated PTAA has lower interface recombination and series resistance, which can explain

the better PV parameters in this device as compared to the device with solution-based PTAA. Using this approach, we also achieve an efficient flexible PSC with PCE of 17.27% and decent flexibility.

Experimental section

Device Fabrication

The ITO glasses were first cleaned by using sonification in different baths for 20 min. The following baths were used for cleaning purpose: Triton X-100 diluted in deionized (DI) water (3 vol%), acetone, and isopropanol. Then, the substrates were treated by oxygen plasma for 10 min before any deposition. After cleaning the substrates were transferred into the thermal evaporation chamber and PTAA with different thickness was thermally evaporated on the substrates with a rate of 0.5 Å/s. For the spin-coated PTAA, a solution of PTAA with a concentration of 2 mg/mL was prepared and spin-coated at 6000 rpm for 40 s, followed by annealing at 150 °C for 10 min. Afterward, $MAPbI_3$ perovskite film was prepared by a layer-by-layer approach as can be found in the literature.[29,30] Briefly, the perovskite was deposited in 10 step by sequentially evaporate PbI_2 and MAI from two separated crucibles. The substrates were put on top of the crucible with a distance of 20 cm. The deposition was performed at a vacuum level of 4×10^{-6} mbar. The PbI_2 and MAI were thermally evaporated at rates of 0.5 nm s^{-1} and 1 nm s^{-1}, respectively. A quartz sensor was used to monitor the thickness for each layer of each layer. The thickness of both layers were calibrated using Alpha-Step 200 (Tencor). After finishing the deposition steps, the perovskite film was annealed at 100 °C for 20 min. Then, C60 (23 nm, as ETL), BCP (8 nm, as buffer layer) and silver (100 nm, back contact) were thermally evaporated on the perovskite film, respectively, through a shadow mask in order to complete the device architecture.

Film characterization

The morphology of the thin films was characterized by a focused ion beam (FIB)-equipped scanning electron microscopy (Helios) and atomic force microscopy (Veeco Dimension 3100). X-ray diffraction (XRD) was recorded by Bruker D8 X-ray Diffractometer (USA). The optical properties of the film

were studied by a Varian Cary 5 for UV-visible measurement and a Fluorolog 322 Horiba Jobin Ybon Ltd for PL characterization. A picosecond pulsed diode laser (EPL-405) was employed to measure the TRPL and for this purpose, the pulse width was 49 ps and the excitation wavelength was 405 nm. The PL lifetime was calculated by using a biexponential equation: ($I(t) = a_i \exp(-t/\tau_i)$), where τ_i and a_i are the lifetime and amplitude for each component, respectively. To study the band alignment, a He I (21.2 eV) photon source was used to record the UPS curves. The measurement was performed by AXIS NOVA (Kratos Analytical Ltd, UK). GPC measurement was performed accordingly: Concentration: 0.1 mg/mL; Injection volume: 100 µL; flow rate: 1 mL/min and temperature was 100 °C.

Device measurement

The J-V curve was recorded by a 2400 Series source meter (Keithley, USA) instrument under AM 1.5G standard condition (100 mW cm^{-2}) using a sun simulator (a xenon lamp with 450 W (Oriel, USA)). The device area was fixed using a shadow mask during the measurement. During the measurement, the voltage scan rate was set to 10 mV/s. The EQE spectra were measured by an Oriel QE-PV-SI (Newport Corporation) with a constant white light bias (5 mW cm^{-2}). The stability of the PSCs was monitored by measuring the MPP of the device in a nitrogen glovebox under continues illumination using an LED lamp with 1 sun power. For EIS measurement, Solartron Analytical setup was employed, and the measurement was performed with zero bias under dark condition. The frequency was changed in the range of 200 mHz-1 MHz in this measurement.

Supporting Information

Supporting Information is available from the Wiley Online Library or from the author.

Acknowledgements

This work was supported by Iran National Science and Technology Foundation (INSF, grant number: 96016250), Iran National Elites Foundation, and Iran Nanotechnology Innovation Council.

M.M.T would like to acknowledge the research laboratory of electronics (RLE) at Massachusetts Institute of Technology (MIT).

Conflict of Interest

The authors declare no conflict of interest.

References

1. M. M. Tavakoli, W. Tress, J. V. Milić, D. Kubicki, L. Emsley, M. Grätzel, *Energy Environ. Sci.* **2018,** *11*, 3310.

2. X. Zheng, B. Chen, J. Dai, Y. Fang, Y. Bai, Y. Lin, H. Wei, X. C. Zeng, J. Huang, *Nat. Energy*, **2017**, *2*, 17102.

3. M. Stolterfoht, C. M. Wolff, J. A. Márquez, S. Zhang, C. J. Hages, D. Rothhardt, S. Albrecht, P. L. Burn, P. Meredith, T. Unold, D. Neher, *Nat. Energy*, **2018**, *3*, 847.

4. M. M. Tavakoli, A. Waleed, L. Gu, D. Zhang, R. Tavakoli, B. Lei, W. Su, F. Fang, Z. Fan, *Nanoscale*, **2017**, *9*, 5828-5834.

5. A. Waleed, M. M. Tavakoli, L. Gu, S. Hussain, D. Zhang, S. Poddar, Z. Wang, R. Zhang, Z. Fan, *Nano lett.* **2017**, *17*, 4951-4957.

6. P. Yadav, S. H. Turren-Cruz, D. Prochowicz, M. M. Tavakoli, K. Pandey, S. M. Zakeeruddin, M. Grätzel, A. Hagfeldt, M. Saliba, *J. Phys. Chem. C*, **2018**, *122*, 15149-15154.

7. M. M. Tavakoli, S. M. Zakeeruddin, M. Grätzel, Z. Fan, *Adv. Mater.* **2018,** *30*, 1705998.

8. D. Luo, W. Yang, Z. Wang, A. Sadhanala, Q. Hu, R. Su, R. Shivanna, G. F. Trindade, J. F. Watts, Z. Xu, T. Liu, K. Chen, F. Ye, P. Wu, L. Zhao, J. Wu, Y. Tu, Y. Zhang, X. Yang, W. Zhang, R. H. Friend, Q. Gong, H. J. Snaith, R. Zhu, *Science*, **2018**, *360*, 1442-1446.

9. M. M. Tavakoli, P. Yadav, R. Tavakoli, J. Kong, *Adv. Energy Mater.* **2018,** *8*, 1800794.

10. M. M. Tavakoli, M. Saliba, P. Yadav, P. Holzhey, A. Hagfeldt, S. M. Zakeeruddin, M. Grätzel, *Adv. Energy Mater.* **2019**, *9*, 1802646.

11. N. J. Jeon, J. H. Noh, W. S. Yang, Y. C. Kim, S. Ryu, J. Seo, S. I. Seok, *Nature*, **2015**, *517*, 476.

12. M. M. Tavakoli, D. Bi, L. Pan, A. Hagfeldt, S.M. Zakeeruddin, M. Grätzel, *Adv. Energy Mater.* **2018,** *8*, 1800275.

13. M. Yavari, M. Mazloum-Ardakani, S. Gholipour, M. M. Tavakoli, S. H. Turren-Cruz, N. Taghavinia, M. Grätzel, A. Hagfeldt, M. Saliba, *Adv. Energy Mater.* **2018**, *8*, 1800177.
14. Q. Zhang, M. M. Tavakoli, L. Gu, D. Zhang, L. Tang, Y. Gao, J. Guo, Y. Lin, S. F. Leung, S. Poddar, Y. Fu, *Nat. Commun.* **2019**, *10*, 727.
15. A. Mahapatra, D. Prochowicz, M. M. Tavakoli, S. Trivedi, P. Kumar, P. Yadav, *J. Mater. Chem. A* 2019, doi:10.1039/C9TA07657C.
16. M. M. Tavakoli, R. Tavakoli, P. Yadav, J. Kong, *J. Mater. Chem. A* **2019**, *7*, 679-686.
17. T. Li, Y. Pan, Z. Wang, Y. Xia, Y. Chen, W. Huang, J. *Mater. Chem. A,* **2017**, *5*, 12602-12652.
18. D. Prochowicz, R. Runjhun, M. M. Tavakoli, P. Yadav, M. Saski, A. Q. Alanazi, D. J. Kubicki, Z. Kaszkur, S. M. Zakeeruddin, J. Lewiński, M. Grätzel, *Chem. Mater.* **2019**, *31*, 1620-1627.
19. National Center for Photovoltaics (NCPV) at the National Renewable Energy Laboratory (NREL); www.nrel.gov/pv/assets/images/efficiency-chart.png.
20. M. M. Tavakoli, R. Tavakoli, S. Hasanzadeh, M. H. Mirfasih, *J. Phys. Chem. C* **2016**, *120*, 19531-19536.
21. Q. Ma, S. Huang, X. Wen, M. A. Green, A. W. Ho-Baillie, *Adv. Energy Mater.* **2016**, *6*, 1502202.
22. M. M. Tavakoli, F. Giordano, S. M. Zakeeruddin, M. Grätzel, *Nano Lett.* **2018**, *18*, 2428–2434.
23. L. Gu, M. M. Tavakoli, D. Zhang, Q. Zhang, A. Waleed, Y. Xiao, K. H. Tsui, Y. Lin, L. Liao, J. Wang, Z. Fan, *Adv. Mater.* **2016**, *28*, 9713-9721.
24. W. Ke, D. Zhao, C. R. Grice, A. J. Cimaroli, G. Fang, Y. Yan, *J. Mater. Chem. A*, **2015**, *3*, 23888-23894.
25. M. M. Tavakoli, R. Tavakoli, Z. Nourbakhsh, A. Waleed, U. S. Virk, Z. Fan, *Adv. Mater. Interfaces* **2016**,*3*,1500790.
26. M. M. Tavakoli, L. Gu, Y. Gao, C. Reckmeier, J. He, A. L. Rogach, Y. Yao, Z. Fan, *Sci. Rep.* **2015,** *5*, 14083.
27. M. Liu, M. B. Johnston, H. J. Snaith, *Nature*, **2013**, *501*, 395–398.
28. M. M. Tavakoli, K. H. Tsui, Q. Zhang, J. He, Y. Yao, D. Li, Z. Fan, *ACS Nano*, **2015**, *9*, 10287-10295.
29. M. M. Tavakoli, P. Yadav, D. Prochowicz, R. Tavakoli, M. Saliba, *J. Phys. D Appl. Phys.* **2018**, *52*, 034005.
30. M. M. Tavakoli, A. Simchi, X. Mo, Z. Fan, *Mater. Chem. Front.* **2017*, 1,*** 1520-1525.
31. J. Ávila, C. Momblona, P. P. Boix, M. Sessolo, H. J. Bolink, *Joule*, **2017**, *1,* 431–442.

32. Z. H. Zheng, H. B. Lan, Z. H. Su, H. X. Peng, J. T. Luo, G. X. Liang, P. Fan, *Sci. Rep.* **2019**, *9*, 1-9.

33. R. Kottokkaran, H. A. Gaonkar, H. A. Abbas, M. Noack, V. Dalal, *J. Mater. Sci. Mater. Electron.* **2019**, *30*, 5487-5494.

34. M. M. Tavakoli, A. Simchi, Z. Fan, H. Aashuri, *Chem. Commun.* **2016**, *52*, 323-326.

35. S. Wang, X. Li, J. Wu, W. Wen, Y. Qi, *Curr. Opin. Electrochem.* **2018**, *11*, 130-140.

36. M. M. Tavakoli, Q. Lin, S. F. Leung, G. C. Lui, H. Lu, L. Li, B. Xiang, Z. Fan, *Nanoscale*, **2016**, *8*, 4276–4283.

37. J. Zhao, R. Tavakoli, M. M. Tavakoli, *Chem. Commun.* 2019, *55*, 9196-9199.

38. M. H. Gharahcheshmeh, M. M. Tavakoli, E. F. Gleason, M. T. Robinson, J. Kong, K. K. Gleason, *Sci. Adv.* **2019**, *5*, eaay0414.

39. M. M. Tavakoli, H. T. Dastjerdi, D. Prochowicz, P. Yadav, R. Tavakoli, M. Saliba, Z. Fan, J. *Mater. Chem. A*, **2019**, *7*, 14753-14760.

40. M. M. Tavakoli, H. T. Dastjerdi, J. Zhao, K. E. Shulenberger, C. Carbonera, R. Po, A. Cominetti, G. Bianchi, N. D. Klein, M. G. Bawendi, S. Gradecak, J. Kong, *Small*, **2019**, *15*, 1900508.

41. S.-Y. Hsiao, H.-L. Lin, W.-H. Lee, W.-L. Tsai, K.-M. Chiang, W.-Y. Liao, C.-Z. Ren-Wu, C.-Y. Chen, H.-W. Lin, *Adv. Mater.* **2016**, *28*, 7013-7019.

42. L. Gil-Escrig, C. Momblona, M. G. La-Placa, P. P. Boix, M. Sessolo, H. J. Bolink, *Adv. Energy Mater.* **2018**, *8*, 1703506.

43. G. Longo, C. Momblona, M.-G. La-Placa, L. Gil-Escrig, M. Sessolo, H. J. Bolink, *ACS Energy. Lett.* **2018**, *3*, 214−219.

44. M. M. Tavakoli, R. Po, G. Bianchi, A. Cominetti, C. Carbonera, N. Camaioni, F. Tinti, J. Kong, *PNAS*, **2019**, *116*, 22037-22043.

45. M. M. Tavakoli, J. Zhao, R. Po, G. Bianchi, A. Cominetti, C. Carbonera, J. Kong, *Adv. Funct. Mater.* **2019**, 1905887.

46. D. Prochowicz, M. M. Tavakoli, A. Solanki, T. W. Goh, K. Pandey, T. C. Sum, M. Saliba and P. Yadav, *J. Mater. Chem. A*, **2018**, *6*, 14307–14314.

47. M. M.Tavakoli, P. Yadav, D. Prochowicz, M. Sponseller, A. Osherov, V. Bulović, J. Kong, *Adv. Energy Mater.* **2019**, *9*, 1803587.

48. T. Golubev, D. Liu, R. Lunt, P. Duxbury, *AIP Adv.* **2019**, *9*, 035026.

49. A. Solanki, M. M. Tavakoli, Q. Xu, S. S. Dintakurti, S. S. Lim, A. Bagui, J. V. Hanna, J. Kong, T. C. Sum, *Adv. Mater.* **2020**, *32*, 1907864.

50. D. Prochowicz, M. M. Tavakoli, A. Solanki, T. W. Goh, T. C. Sum, P. Yadav, *J. Mater. Chem. C*, **2019**, *7*, 1273-1279.

51. M. M. Tavakoli, D. Prochowicz, P. Yadav, R. Tavakoli and M. Saliba, *Eng. Sci.*, **2018**, *3*, 48-53.

TOC

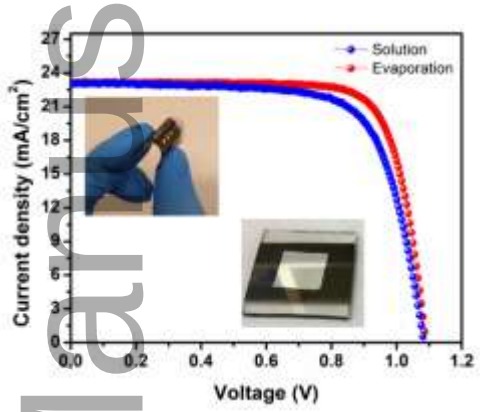

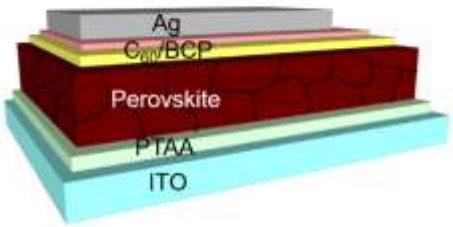

In this study, all-vacuum processed inverted perovskite solar cells were developed by thermal evaporation of PTAA, resulted in efficiencies of 19.4% and 17.27% for rigid and flexible devices, respectively.